









Dye Elimination by Surface-Functionalized Magnetite Nanoparticles: Kinetic and Isotherm Studies

Arti Jangra¹, Jaiveer Singh¹, Jai Kumar¹, Keerti Rani¹, Parvin Kumar¹,
Suresh Kumar¹, Devender Singh² and Ramesh Kumar^{1,*}

¹ Department of Chemistry, Kurukshetra University, Kurukshetra (Haryana), 136119, India; aj4410@gmail.com (A.J.), jaiveersinghkuk@gmail.com (J.S.), jaikumarbrwl@gmail.com (J.K.), keertiattri150@gmail.com (K.R.), parvinjangra@gmail.com (P.K.), duaskchem@gmail.com (S.K.), and rameshkumarkuk@gmail.com (R.K.);

² Department of Chemistry, Maharshi Dayanand University, Rohtak (Haryana), 124001, India; devjakhar@gmail.com (D.S.);

* Correspondence e-mail: rameshkumarkuk@gmail.com, rameshchemkuk@kuk.ac.in (R.K.);

Received: 19.05.2022; Accepted: 23.07.2022; Published: 11.09.2022

Abstract: In the present manuscript, uncoated and citric acid-coated magnetic nanoparticles were synthesized and characterized using various techniques. The manuscript mainly focuses on the adsorption study of the citric acid-modified magnetic nanoparticles for dye adsorption from the solution. The effect of several factors, including adsorbent amount, adsorption time, and dye solution concentration, were examined. Additionally, kinetic and isotherm studies confirmed that the adsorption process followed pseudo-second-order kinetics and the Langmuir isotherm model. The desorption study was also scrutinized. The coated magnetite nanoparticles show better adsorption capacity than uncoated magnetite nanoparticles.

Keywords: adsorption; citric acid; magnetite nanoparticles; co-precipitation.

© 2022 by the authors. This article is an open-access article distributed under the terms and conditions of the Creative Commons Attribution (CC BY) license (<https://creativecommons.org/licenses/by/4.0/>).

1. Introduction

Industrialization is considered to be the key to economic growth. Besides this, it is also considered to be the basic reason for environmental pollution. Several dyes are non-biodegradable, toxic, carcinogenic, and mutagenic. Thus, the discharge of effluents with dye residues into natural water streams such as rivers is a serious environmental concern because of their adverse effects on humans and aquatic life. Predominantly, among various dyes classification, the maximum toxicity is accompanied by cationic dyes such as Crystal violet and Safranin-O. These pollutants can also cause allergic eczema, cancer, mutations, and skin aggravations[1]. Thus, treating water with dye residues before being discharged into the water streams becomes environmentally important to control water pollution. Numerous methods, including photolytic degradation[2], biological treatment[3], adsorption[4], electrochemical [5], exchange membrane [6], chemical oxidation[7], flocculation[8], etc., have been established for the adsorption of dye pollutants[9] from aqueous solution. Among these techniques, the adsorption process is referred to as an efficient, easy, and appropriate approach due to its economic feasibility, high efficiency, and capability to separate an extensive range of industrial pollutants, including various dye pollutants. Numerous adsorbents, such as bamboo activated carbon[10], orange peel powder[11], clay[12], cotton[13], etc., have been examined for the removal of dyes from an aqueous solution. Moreover, these adsorbents are restricted due to difficulty in separation or less efficient adsorption capabilities. So, the adsorbents with high

adsorption capacity and easy separation capability are considered efficient adsorbents. Thus, nanotechnology is considered an attractive approach to overcoming these problems. In addition to this, magnetic nanoparticles have been used as promising adsorbents for the adsorption of pollutants owing to their unique magnetic properties, easy separability, large surface area to volume ratio, and recyclability. Bare magnetic nanoparticles agglomerate easily, which may affect their adsorption capability. Several pieces of research focused on the modification of bare magnetic nanoparticles have been reported. For this purpose, numerous natural or synthetic materials, such as poly-acrylic[14,15], polyaniline[16], chitosan[17], sodium alginate[18], etc., have been used to modify the surface of bare magnetic nanoparticles. In the present manuscript, citric acid-modified magnetic nanoparticles were synthesized and utilized as a promising adsorbent to remove the crystal violet dye from an aqueous solution.

2. Materials and Methods

2.1. Materials.

Ferric chloride hexahydrate ($\text{FeCl}_3 \cdot 6\text{H}_2\text{O}$), Ferrous sulfate heptahydrate ($\text{FeSO}_4 \cdot 7\text{H}_2\text{O}$, 98%), ammonium hydroxide solution (25%), Crystal Violet (CV) dye and citric acid (CA) were purchased from SRL (India) and used without any further purification.

2.2. Characterization techniques.

The infrared spectra of uncoated magnetite nanoparticles (Fe_3O_4) and CA-modified magnetite nanoparticles ($\text{CA}@\text{Fe}_3\text{O}_4$), as well as pure CA, were obtained in the range 500-4000 cm^{-1} using the MBB-3000 ABB (Fourier transformation infrared) FTIR spectrometer to identify the functional groups. The thermal analysis of nanoparticles was carried out by Perkin Elmer STA-6000 thermogravimetric analyzer under optimum conditions (heating rate 5-80°C/min and 20-1000°C temperature range). The X-ray diffraction (XRD) pattern of synthesized nanoparticles was recorded on a diffractometer equipped with Cu $K\alpha$ radiations ($\lambda = 1.540 \text{ \AA}$) over a 2θ range of 20°-80° at room temperature. Both Hitachi SU-8000 field emission scanning electron microscope (FESEM) and Microtrac W3602 particle size analyzer was used to observe the average size of synthesized magnetic nanoparticles. Fe_3O_4 and $\text{CA}@\text{Fe}_3\text{O}_4$ magnetic nanoparticles were dispersed in water using an ultra-sonicator to determine their average size and size distribution. A T90 PG instrument limited UV-visible spectrophotometer (900-190 nm) was used for absorbance measurements.

2.3. Synthesis of uncoated and coated citric acid magnetite nanoparticles.

In the present work, the co-precipitation method was used to synthesize magnetic nanoparticles. Briefly, 4.2 g of $\text{FeSO}_4 \cdot 7\text{H}_2\text{O}$ and 6.1 g of $\text{FeCl}_3 \cdot 6\text{H}_2\text{O}$ were dissolved in 100 mL of de-ionized water. The solution was heated up to 90°C, followed by the quick addition of 10 mL of ammonium hydroxide (25%). The black-colored uncoated magnetite nanoparticles (Fe_3O_4) were formed. The 10 mL of citric acid (0.5 g/mL) was added for the surface functionalization of uncoated magnetic nanoparticles and stirred for an extra 30 min[19]. Then these coated magnetic nanoparticles were separated by applying an external magnetic field.

2.4. Adsorption analysis.

Batch adsorption studies of CA-modified magnetite nanoparticles were performed for the adsorption of CV dye from an aqueous solution at room temperature. Several studies were carried out to examine the effects of various factors, including the concentration of dye (05-20 mg/L), adsorbent amount (5-30 mg), and contact time (0-40 min) on the adsorption of crystal violet dye. The effect of contact time helps to determine the equilibrium time for the adsorption of CV dye. Moreover, the effect of the concentration of CV dye was studied at equilibrium time using a fixed amount of adsorbent (05 mg). The absorbance of solutions was measured at 587 nm using a UV-Visible spectrophotometer. The amount of CV adsorbed was determined using the mass balance equation (1):

$$q_e = \frac{(C_0 - C_e)V}{m} \quad (1)$$

Where C_0 and C_e are the initial and equilibrium concentrations of CV dye, q_e is the adsorption capacity, V is the volume of solution taken, and m is the mass of adsorbent added. The removal efficiency of CV dye was calculated using the formula (2):

$$\%R = \frac{(C_0 - C_e)}{C_0} \times 100 \quad (2)$$

Various kinetic and isotherm models, including pseudo-first-order [20,21] as well as pseudo-second order [22,23] kinetic equations (Table 1), Langmuir [24,25], Freundlich [26,27], Temkin [28,29] were studied to inspect the adsorption rate of CV dye and interaction mechanism of adsorbent with an adsorbate.

Table 1. General equation of kinetic models of pseudo-first-order and pseudo-second-order kinetic models.

Kinetic Model	Equations
Pseudo-First-Order	$\log(q_e - q_t) = \log q_e - \frac{k_1 t}{2.303}$
Pseudo-second-Order	$\frac{t}{q_t} = \frac{1}{k_2 q_e^2} + \frac{t}{q_e}$

*Where, t = Time, q_e = Adsorption capacity at equilibrium, q_t = Adsorption capacity at time, k_1 = Pseudo- first-order constant, k_2 = Pseudo- second-order constant

2.5. Desorption study.

A desorption experiment was performed to evaluate the reusability of CA@Fe₃O₄ nanoparticles. 30 mg of crystal violet dye-loaded citric acid coated magnetite nanoparticles (CV@CA@Fe₃O₄) nanoparticles were mixed with 30 mL of ethanol and stirred for about 100-120 min at room temperature. Then the magnetic nanoparticles were separated using a magnet, and the absorbance of the decanted solution was measured at 587 nm. The desorption capacity (q_{de}) was calculated using equation (3):

$$q_{de} = \frac{C_{de} V}{m} \quad (3)$$

where C_{de} (mg/L) is the dye concentration in ethanol, V is the volume of ethanol used, and m is the mass of CV@CA@Fe₃O₄ nanoparticles.

And the percentage of desorption efficiency (W_{de}) can be expressed as (4):

$$W_{de} = \frac{q_e}{q_{de}} \times 100 \quad (4)$$

After desorption, the coated nanoparticles were recollected and dried. Additionally, the adsorption capacity of recycled nanoparticles was investigated again to examine the reusability.

3. Results and Discussion

3.1.Characterization.

3.1.1. Fourier transformation infrared (FTIR) analysis.

Comparison of IR spectra of uncoated and CA-modified magnetic nanoparticles and pure CA revealed successful coating on the surface of uncoated magnetic nanoparticles. IR spectrum of uncoated Fe₃O₄ nanoparticles (Figure 1a) showed a prominent peak near 600 cm⁻¹ corresponding to Fe-O stretching, while the band at 3300 cm⁻¹ may be assigned to O-H stretching. The spectrum of pure CA exhibited an intense peak near 1700 cm⁻¹ that may be attributed to the C=O stretching vibration (Figure 1b). In the spectrum of CA-coated magnetic nanoparticles (CA@Fe₃O₄), two new peaks near 1625 and 1425 cm⁻¹ (Figure 1c) were observed, corresponding to asymmetric and symmetric stretching of the carboxylate group of citric acid generated during coating in alkaline medium.

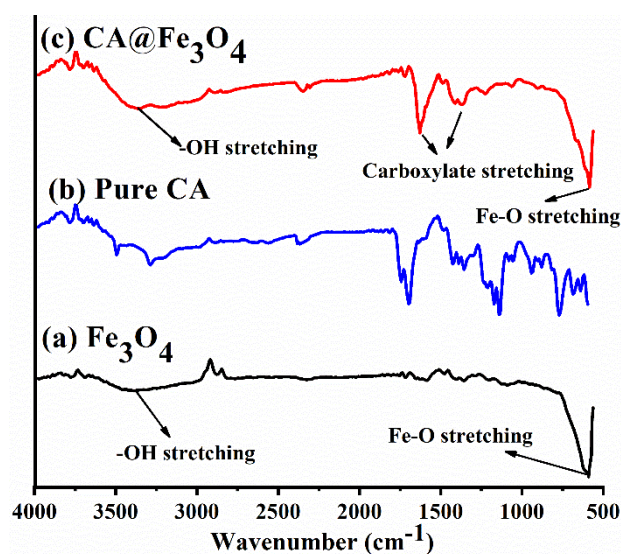


Figure 1. Fourier transformation infrared spectra of uncoated magnetite nanoparticles (a), pure citric acid; (b) citric acid coated magnetite nanoparticles (c).

3.1.2. Field emission scanning electron microscopy (FESEM) study.

FESEM images and the histograms of uncoated and citric acid-coated magnetite nanoparticles demonstrated their respective diameters. The average particle size of 11 nm and 34 nm was observed for uncoated and citric acid-coated magnetite nanoparticles, respectively (Figure 2). The increment in the size of coated magnetic nanoparticles demonstrated the prosperous surface modification of uncoated magnetite nanoparticles.

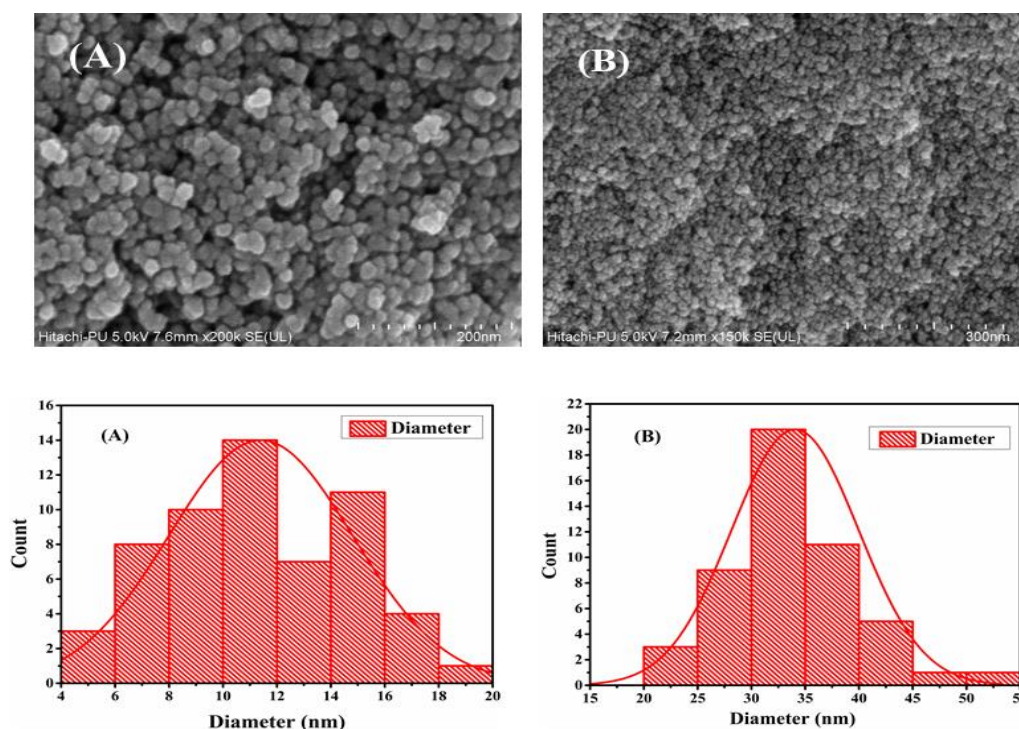


Figure 2. Field emission scanning electron microscope images and histograms of uncoated magnetite nanoparticles (A) [1 division= 20 nm] and citric acid coated magnetite nanoparticles (B) [1 division= 30 nm].

3.1.3. X-ray diffractometer (X-RD) analysis.

The recorded XRD pattern of CA-coated magnetic nanoparticles showed five crystalline peaks, which results in the semi-crystalline nature of synthesized nanoparticles (Figure 3). The Debye-Scherrer equation was used to calculate the mean size of nanoparticles.

$$d = (0.914\lambda / \beta \cos \theta)$$

where, λ is the ray wavelength (1.540 Å), β is full-width at half maximum, and θ is Bragg angle in degree. The calculated diameter for CA-coated magnetic nanoparticles was found to be 32.5 nm, and the results are close to that depicted by FESEM studies.

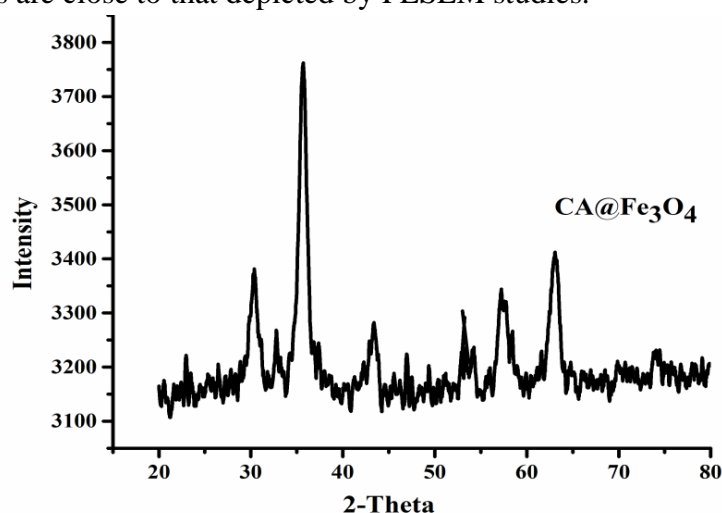


Figure 3. The powder X-ray diffraction of citric acid-coated magnetite nanoparticles.

3.1.4. Thermogravimetric studies.

Thermal gravimetric analysis (TGA) was used to confirm the efficiency of coating and performed under atmospheric conditions. Thermograms exhibited two steps of weight loss for

uncoated Fe_3O_4 nanoparticles and three steps for $\text{CA@Fe}_3\text{O}_4$ nanoparticles (Figure 4). The first weight loss of ~5% occurs between 10-150°C, which corresponds to the loss of water molecules. Moreover, the second weight loss for $\text{CA@Fe}_3\text{O}_4$ between 160-220°C is attributed due to the decomposition of the citric acid-coated layer. The results suggested that $\text{CA@Fe}_3\text{O}_4$ depicts higher thermal stability than pure CA[30]. Additionally, the observed weight loss after 400°C might be related to Fe_3O_4 nanoparticles. The thermo grams illustrated that total weight loss for uncoated Fe_3O_4 and $\text{CA@Fe}_3\text{O}_4$ was ~11.76% and 31.05%, respectively.

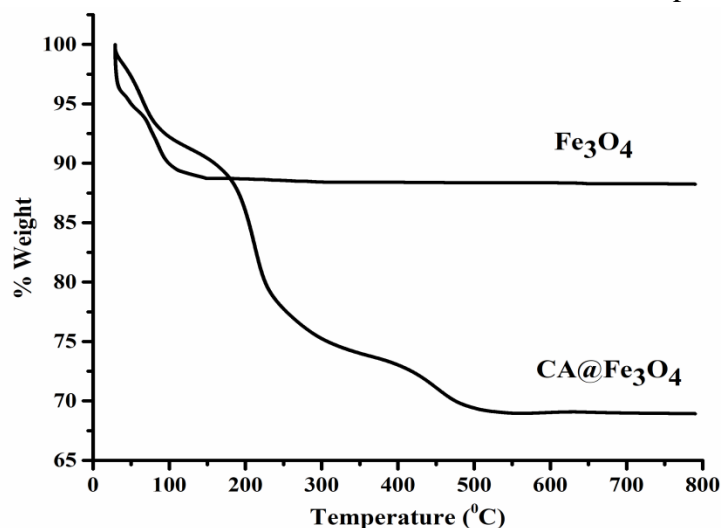


Figure 4. Thermogravimetric curves of uncoated magnetite and citric acid coated magnetite nanoparticles.

3.2. Batch adsorption analysis.

Several sorption experiments were implemented to examine the effects of different adsorption factors, such as the amount of $\text{CA@Fe}_3\text{O}_4$ (05-30 mg) and crystal violet dye concentration (varying from 05 to 20 mg/L), and contact time on the adsorption behavior of $\text{CA@Fe}_3\text{O}_4$.

3.2.1. Effect of adsorbent amount.

$\text{CA@Fe}_3\text{O}_4$ and uncoated magnetite nanoparticles were used as an adsorbent. The effect of the adsorbent amount on the adsorption of crystal violet (CV) dye (20 mg/L) was examined at room temperature and optimum conditions.

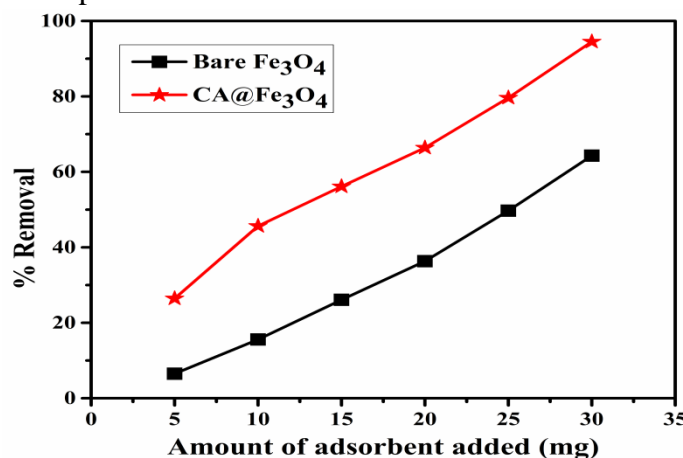


Figure 5. Effect of amount of adsorbent added on percentage removal efficiency for both uncoated and citric acid coated magnetite nanoparticles.

The results suggested that the removal efficiency of crystal violet (CV) dye was increased with the increase in the amount of adsorbent [Figure 5] and the coated magnetite nanoparticles displayed higher percentage removal efficiency of crystal violet dye than uncoated magnetite nanoparticles.

3.2.2. Effect of initial concentration of adsorbate.

The influence of the initial concentration of crystal violet (CV) dye (05-20 mg/L) was investigated under specific conditions such as fixed-dose of adsorbent (5 mg/L), equilibrium time, and 8.3 pH. Moreover, a decrease was observed in increasing the initial concentration of crystal violet (CV) dye. Approximately 48.26 %, 39.17 %, 32.07 % and 26.45 % of removal efficiency were observed for 05 to 20 mg/L crystal violet (CV) dye concentration, respectively.

3.2.3. Kinetic studies and effect of the contact period.

The effect of contact time on the adsorption behavior of CA@Fe₃O₄ was studied using fixed crystal violet dye concentration (20 mg/L). The study revealed that the saturation point was reached after 40 min for both CA@Fe₃O₄ and uncoated Fe₃O₄ magnetite nanoparticles (Figure 6). In addition, two kinetic models, including pseudo-first-order and pseudo-second-order models, were used to investigate the mechanism of the adsorption process (Figure 7).

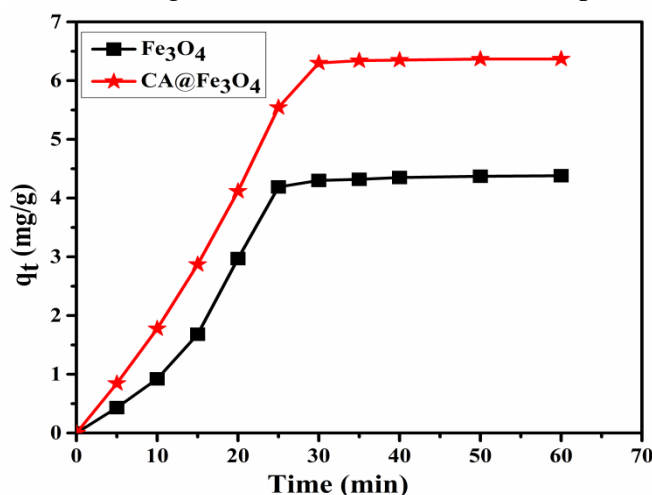


Figure 6. Effect of contact time on the adsorption capacity of both uncoated and citric coated magnetite nanoparticles.

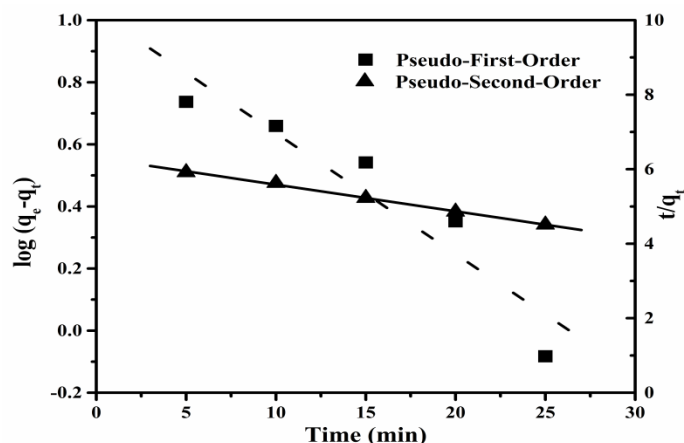


Figure 7. Graph of pseudo-first-order and pseudo-second-order kinetics for citric acid coated magnetite nanoparticles.

The correlation coefficient (R^2) for the pseudo-first-order equation was found to be lower than the pseudo-second-order equation (0.99695), which depicted the chemisorption of crystal violet (CV) dye on the surface of CA@Fe₃O₄. Thus, the study revealed the applicability of pseudo-second-order to define the adsorption process.

3.2.4. Isotherm Analysis.

It is important to establish the most appropriate isotherm model to evaluate the interactions between adsorbate and adsorbent. For this purpose, linearized forms of isotherm models, including Langmuir (5), Freundlich (6), and Temkin (7), were applied respectively to examine the nature of adsorption of crystal violet dye (CV) over the surface of CA@Fe₃O₄. The data depicted that the isotherm study fitted well with the Langmuir isotherm [Figure 8] with a good correlation coefficient, R^2 [Table 2].

$$\frac{C_e}{q_e} = \frac{1}{bq_m} + \frac{C_e}{q_m} \quad (5)$$

$$\log q_e = \log K_F + \frac{1}{n} \log C_e \quad (6)$$

$$q_e = B \ln A + B \ln C_e, B = \frac{RT}{b} \quad (7)$$

where q_m is maximum adsorption capacity, b is Langmuir constant, q_e is loading capacity at equilibrium, K_f is Freundlich constant, A is Temkin constant, R is gas constant, T is temperature, and C_e is equilibrium concentration.

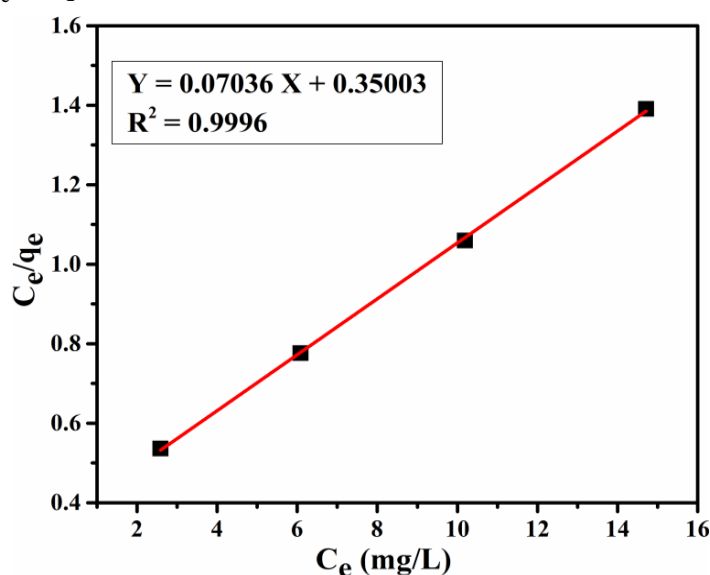


Figure 8. A plot of isotherm model of adsorption process for citric acid coated magnetite nanoparticles.

Table 2. Constants for adsorption isotherm models.

Langmuir			Freundlich			Temkin		
R^2	q_m (mg/g)	K_L (L/mg)	R^2	N	K_F (mg/g)	R^2	A (L/mg)	B (J/mol)
0.9996	14.21	0.21	0.9017	2.18	0.52	0.8961	1.66	3.35

3.3. Desorption results.

The desorption process was performed before reusing CA-coated magnetite nanoparticles. 89.95% of desorption efficiency was obtained. Additionally, no significant

change was observed in the adsorption capacity of recollected CA@Fe₃O₄ nanoparticles, which suggested that these nanoparticles can be reused for the adsorption of CV dye from an aqueous solution.

4. Conclusions

In this study, uncoated Fe₃O₄ and CA-coated Fe₃O₄ nanoparticles were prepared by the co-precipitation method. Then these prepared nanoparticles were characterized using different analyses such as FTIR spectroscopy, Thermal gravimetric analysis (TGA), FESEM, and X-ray diffractometer (XRD). In addition, these were employed as an adsorbent for crystal violet dye adsorption from the aqueous solution. Characterization results depicted the successful coating of CA on the surface of Fe₃O₄ magnetic nanoparticles. The results revealed good adsorption behavior of crystal violet dye onto the surface of CA@Fe₃O₄ nanoparticles, which may be due to the addition of new functional groups of citric acid. The synthesized adsorbents were observed to remove ~ 94.5% of crystal violet (CV) dye from an aqueous solution. The adsorption kinetics and isotherm study agreed well with the pseudo-second-order and Langmuir isotherm model, respectively. The desorption study suggested the reusable properties of these magnetic nanoparticles. Hence, the results illustrated that these synthesized CA@Fe₃O₄ nanoparticles have promising applications in the removal of crystal violet dye from the aqueous solution and can be considered an effective and reusable adsorbent.

Funding

The authors are grateful to UGC, New Delhi, India, for providing financial support in the form of Senior Research Fellowship (SRF); Award No. 115576, 134490, Nov2017-114450.

Acknowledgments

Co-authors Arti Jangra, Jaiveer Singh, and Keerti Rani are highly thankful to Kurukshetra University, Kurukshetra, for providing research facilities.

Conflicts of Interest

The authors declare no conflict of interest.

References

1. Vishnu, D.; Dhandapani, B.; Authilingam, S.; Sivakumar, S.V. A Comprehensive Review of Effective Adsorbents Used for the Removal of Dyes from Wastewater. *Curr. Anal. Chem.* **2020**, *18*, 255, <https://doi.org/10.2174/1573411016999200831111155>.
2. Rahman, A.; Rahman, A. Silver Oxide-Decorated Silica Nanoparticles for Visible-Light-Driven Photolytic Pollutant Degradation and Water–Oil Separation. *ACS Appl. Nano Mater.* **2022**, *5*, 939, <https://doi.org/10.1021/acsanm.1c03606>.
3. Tawfik, A.; Bakr, M.H.; Nasr, M.; Haider, J.; Mesfer, M.K. A.; Lim, H.; Qyyum, M.A.; Lam, S.S. Economic and Environmental Sustainability for Anaerobic Biological Treatment of Wastewater from Paper and Cardboard Manufacturing Industry. *Chemosphere* **2022**, *289*, 133166, <https://doi.org/10.1016/j.chemosphere.2021.133166>.
4. Soh, E.Y.S.; Lim, S.S.; Chew, K.W.; Phuang, X.W.; Ho, V.M.V.; Chu, K.Y.H.; Wong, R.R.; Lee, L.Y.; Tiong, T.J. Valorization of Spent Brewery Yeast Biosorbent with Sonication-Assisted Adsorption for Dye Removal in Wastewater Treatment. *Environ. Res.* **2022**, *204*, 112385, <https://doi.org/10.1016/j.envres.2021.112385>.

5. Hao, Y.; Ma, H.; Proietto, F.; Galia, A.; Scialdone, O. Electrochemical Treatment of Wastewater Contaminated by Organics and Containing Chlorides: Effect of Operative Parameters on the Abatement of Organics and the Generation of Chlorinated by-Products. *Electrochim. Acta***2022**, *402*, 139480, <https://doi.org/10.1016/j.electacta.2021.139480>.
6. Sugioka, M.; Yoshida, N.; Yamane, T.; Kakihana, Y.; Higa, M.; Matsumura, T.; Sakoda, M.; Iida, K. Long-Term Evaluation of an Air-Cathode Microbial Fuel Cell with an Anion Exchange Membrane in a 226L Wastewater Treatment Reactor. *Environ. Res.***2022**, *205*, 112416, <https://doi.org/10.1016/j.envres.2021.112416>.
7. Wang, J.; Li, M.; Guan, A.; Liu, R.; Qi, W.; Liu, H.; Qu, J. Can Radicals-Orientated Chemical Oxidation Improve the Reduction of Antibiotic Resistance Genes (ARGs) by Mesophilic Anaerobic Digestion of Sludge. *J. Hazard. Mater.***2022**, *426*, 128001, <https://doi.org/10.1016/j.jhazmat.2021.128001>.
8. Abujazar, M.S.S.; Karaağaç, S.U.; Abu Amr, S.S.; Alazaiza, M.Y.D.; Bashir, M.J. Recent Advancement in the Application of Hybrid Coagulants in Coagulation-Flocculation of Wastewater: A Review. *J. Clean. Prod.***2022**, *345*, 131133, <https://doi.org/10.1016/j.jclepro.2022.131133>.
9. Tao, D.; Higaki, Y.; Ma, W.; Takahara, A. Halloysite Nanotube/Polyelectrolyte Hybrids as Adsorbents for the Quick Removal of Dyes from Aqueous Solution. *Chem. Lett.***2015**, *44*, 1572, <https://doi.org/10.1246/cl.150727>.
10. Agbor Tabi, G.; Ngouateu Rene Blaise, L.; Daouda, K.; Naphtali Odogu, A.; Aime Victoire, A.; Nsami Julius, N.; Joseph Mbadcam, K. Non-Linear Modelling of the Adsorption of Indigo Carmine Dye from Wastewater onto Characterized Activated Carbon/Volcanic Ash Composite. *Arab. J. Chem.***2022**, *15*, 103515, <https://doi.org/10.1016/j.arabjc.2021.103515>.
11. Szepesi, G.L.; Szamosi, Z.; Zhang, W.; Wang, Y.; Fan, L.; Liu, X.; Cao, W.; Ai, H.; Wang, Z.; Liu, X.; *et al.* Sorbent Properties of Orange Peel-Based Biochar for Different Pollutants in Water. *Process.* **2022**, *10*, 856, <https://doi.org/10.3390/pr10050856>.
12. Wang, Z.K.; Li, T.T.; Peng, H.K.; Ren, H.T.; Lin, J.H.; Lou, C.W. Natural-Clay-Reinforced Hydrogel Adsorbent: Rapid Adsorption of Heavy-Metal Ions and Dyes from Textile Wastewater. *Water Environ. Res.***2022**, *94*, 10698, <https://doi.org/10.1002/wer.10698>.
13. Abdelhameed, R.M.; Emam, H.E. Modulation of Metal Organic Framework Hybrid Cotton for Efficient Sweeping of Dyes and Pesticides from Wastewater. *Sustain. Mater. Technol.***2022**, *31*, 00366, <https://doi.org/10.1016/j.susmat.2021.e00366>.
14. Ling, C.; Yimin, D.; Qi, L.; Chengqian, F.; Zhiheng, W.; Yaqi, L.; Ling, C.; Bo, L.; Yue-fei, Z.; Yan, L.; *et al.* Fabrication of Magnetic Targeted Cellulose/Poly (Acrylic Acid-Co-2-Methacryloyloxyethyl Trimethylammonium Chloride) Composites for Adsorbing Congo Red Dye from Aqueous Solution. *J. Mater. Sci. Mater. Electron.***2022**, *33*, 5750, <http://doi.org/10.1007/s10854-022-07760-6>.
15. Hosseini, H.; Zirakjou, A.; McClements, D.J.; Goodarzi, V.; Chen, W.H. Removal of Methylene Blue from Wastewater Using Ternary Nanocomposite Aerogel Systems: Carboxymethyl Cellulose Grafted by Polyacrylic Acid and Decorated with Graphene Oxide. *J. Hazard. Mater.***2022**, *421*, 126752, <https://doi.org/10.1016/j.jhazmat.2021.126752>.
16. Lyu, W.; Li, J.; Trchová, M.; Wang, G.; Liao, Y.; Bober, P.; Stejskal, J. Fabrication of Polyaniline/Poly(Vinyl Alcohol)/Montmorillonite Hybrid Aerogels toward Efficient Adsorption of Organic Dye Pollutants. *J. Hazard. Mater.***2022**, *435*, 129004, <https://doi.org/10.1016/j.jhazmat.2022.129004>.
17. Saheed, I.O.; Oh, W. Da; Suah, F.B.M. Chitosan Modifications for Adsorption of Pollutants – A Review. *J. Hazard. Mater.***2021**, *408*, 124889, <https://doi.org/10.1016/j.jhazmat.2020.124889>.
18. Maqbool, M.; Sadaf, S.; Bhatti, H.N.; Rehmat, S.; Kausar, A.; Alissa, S.A.; Iqbal, M. Sodium Alginate and Polypyrrole Composites with Algal Dead Biomass for the Adsorption of Congo Red Dye: Kinetics, Thermodynamics and Desorption Studies. *Surfaces and Interfaces***2021**, *25*, 101183, <https://doi.org/10.1016/j.surfin.2021.101183>.
19. Singh, D.; Gautam, R.K.; Kumar, R.; Shukla, B.K.; Shankar, V.; Krishna, V. Citric Acid Coated Magnetic Nanoparticles: Synthesis, Characterization and Application in Removal of Cd(II) Ions from Aqueous Solution. *J. Water Process Eng.***2014**, *4*, 233, <https://doi.org/10.1016/j.jwpe.2014.10.005>.
20. Langergren, S., and Svenska, B. Zur Theorie Der Sogenannten Adsorption Geloester Stoffe. *Veternskapsakad. Handlingar***1898**, *24*, 1.
21. Ghibate, R.; Senhaji, O.; Taouil, R. Kinetic and Thermodynamic Approaches on Rhodamine B Adsorption onto Pomegranate Peel. *Case Stud. Chem. Environ. Eng.***2021**, *3*, 100078, <https://doi.org/10.1016/j.cscee.2020.100078>.

22. Ho, Y.S.; McKay, G. Pseudo-Second Order Model for Sorption Processes. *Process Biochem.***1999**, *34*, 451, [https://doi.org/10.1016/S0032-9592\(98\)00112-5](https://doi.org/10.1016/S0032-9592(98)00112-5).
23. Priyadarshini, B.; Patra, T.; Sahoo, T.R. An Efficient and Comparative Adsorption of Congo Red and Trypan Blue Dyes on MgO Nanoparticles: Kinetics, Thermodynamics and Isotherm Studies. *J. Magnes. Alloy.***2021**, *9*, 478, <https://doi.org/10.1016/j.jma.2020.09.004>.
24. Langmuir, I. The Adsorption of Gases on Plane Surfaces of Glass, Mica and Platinum. *J. Am. Chem. Soc.***1918**, *40*, 1361, <https://doi.org/10.1021/ja02242a004>.
25. Al-Trawneh, S.A.; Jiries, A.G.; Alshahateet, S.F.; Sagadevan, S. Phenol Removal from Aqueous Solution Using Synthetic V-Shaped Organic Adsorbent: Kinetics, Isotherm, and Thermodynamics Studies. *Chem. Phys. Lett.***2021**, *781*, 138959, <https://doi.org/10.1016/j.cplett.2021.138959>.
26. Freundlich, H. Über Die Adsorption in Lösungen. *Zeitschrift für Phys. Chemie***1907**, *57U*, 385, <https://doi.org/10.1515/zpch-1907-5723>.
27. İsmail, O.; Gökçe Kocabay, Ö. Absorption and Adsorption Studies of Polyacrylamide/Sodium Alginate Hydrogels. *Colloid Polym. Sci.***2021**, *299*, 783, <https://doi.org/10.1007/s00396-020-04796-0>.
28. Temkin, M.J. Pyzhev, V. Recent Modifications to Langmuir Isotherms, *Acta Physiochim. Ussr.***1940**, *12*, 217.
29. Elemile, O.O.; Akpor, B.O.; Ibitogbe, E.M.; Afolabi, Y.T.; Ajani, D.O. Adsorption Isotherm and Kinetics for the Removal of Nitrate from Wastewater Using Chicken Feather Fiber. *Cogent Eng.* **2022**, *9*, 2043227, <https://doi.org/10.1080/23311916.2022.2043227>.
30. Goodarzi, A.; Sahoo, Y.; Swihart, M.T.; Prasad, P.N. Aqueous Ferrofluid of Citric Acid Coated Magnetite Particles. In *Proceedings of the Materials Research Society Symposium - Proceedings*,**2003**, 789, 129, <https://doi.org/10.1557/PROC-789-N6.6>.